

Date of publication xxxx 00, 0000, date of current version xxxx 00, 0000.

Digital Object Identifier 10.1109/ACCESS.2017.DOI

# Deep Learning for Path Loss Prediction at 7 GHz in Urban Environment

THAO T. NGUYEN<sup>1</sup>, NADIA YOZA-MITSUISHI<sup>2</sup>, AND RAIED CAROMI<sup>3</sup>.

<sup>1</sup>National Institute of Standards and Technology, Gaithersburg, MD 20899 USA (e-mail: thao.t.nguyen@nist.gov)

<sup>2</sup>National Institute of Standards and Technology, Boulder, CO 80305 USA (e-mail: nadia.yozamitsuishi@nist.gov)

<sup>3</sup>National Institute of Standards and Technology, Gaithersburg, MD 20899 USA (e-mail: raied.caromi@nist.gov)

Corresponding author: Thao T. Nguyen (e-mail: thao.t.nguyen@nist.gov).

This work was supported by the U.S. National Institute of Standards and Technology, Communications Technology Laboratory. U.S. Government work not subject to U.S. copyright.

**ABSTRACT** In the 6 GHz spectrum sharing band, unlicensed devices are managed by automated frequency coordination (AFC) systems to protect incumbent services from interference. Thus, it is important to select accurate propagation models for interference calculation and analysis. This paper utilizes a model-aided deep learning technique for path loss prediction at 7 GHz, as a representative frequency within the 6 GHz band, in an urban environment. The proposed model is a hybrid model, which leverages both domain expert knowledge from a physics-based general-purpose channel model as well as the learning-based capability from a neural network, for path loss prediction. The model is trained and tested using sufficient-quantity and high-quality real propagation measurement data collected in four locations in an urban environment. Numerical results show that the deep learning model provides a better prediction performance than most empirical models. Furthermore, the feasibility of proposed model generalization to new locations after fine-tuning is examined.

**INDEX TERMS** Deep learning, path loss prediction, propagation model, spectrum sharing.

## I. INTRODUCTION

THE ever increasing demand for more radio-frequency (RF) spectrum to support high capacity, gigabit speeds, and low latency wireless communications in fifth-generation (5G) and upcoming sixth-generation (6G) is inevitable. One of the promising solutions to tackle the spectrum bottleneck problem is spectrum sharing technology, which can create more opportunities for commercial services while protecting incumbents from harmful interference.

In April 2020, the U.S. Federal Communications Commission (FCC) adopted a Report and Order authorizing the 6 GHz band (5.925 to 7.125) GHz to be shared between unlicensed uses and current incumbents, including fixed microwave links [1]. Two types of unlicensed devices are specified in the report including standard-power access points and low-power access points. The standard-power access points operate under the control of an automated frequency coordi-

ination (AFC)<sup>1</sup> system to protect the incumbent microwave receivers from harmful interference. Among many functional and operational requirements, the AFC needs to utilize accurate propagation models in order to effectively compute the interference link budget at the incumbent receiver. After evaluating different propagation models, the FCC has suggested to use a combination of i) the free-space path loss model for distances up to 30 m, ii) the Wireless World Initiative New Radio phase II (WINNER II) for distances up to 1 km along with buildings and terrain data for determining line-of-sight (LOS) and non-line-of-sight (NLOS) path losses, and iii) Irregular Terrain Model (ITM) combined with the appropriate clutter model (e.g., International Telecommunication Union (ITU)-R P.2108 for urban and suburban, ITU-R P.452 for rural) for distances greater than 1 km. Although the models have been proposed by the FCC, several parameters used in these models have not been determined. The Wireless

<sup>1</sup>Certain commercial equipment, instruments, or materials are identified in this paper to foster understanding. Such identification does not imply recommendation or endorsement by the National Institute of Standards and Technology, nor does it imply that the materials or equipment identified are necessarily the best available for the purpose.

Innovation Forum (WInnForum) 6 GHz Committee has been working on the propagation parameters to be included in the AFC functional requirements [2].

Propagation modeling has been an intriguing yet contentious research area in the wireless community. Numerous models have been developed for different environments and conditions in different frequency bands. The developed models can be classified as purely theoretical models, empirically (and statistically) fitted models, deterministic ray-tracing models, or combination thereof. In recent years, with the advancements of machine learning (ML) and deep learning (DL) technology, researchers have been applying these techniques into the path loss prediction problem. Because these ML/DL models are trained on a large amount of real measurement data, they tend to provide better performance accuracy than most traditional propagation models.

In this paper, we aim to apply a DL technique to predict the path loss at 7 GHz in an urban environment. The main contributions of our work include:

- Enhancements to the model-aided DL models developed in [20], [22] for path loss prediction at 7 GHz as a representative frequency within the 6 GHz band.
- Utilizing the real propagation measurement data collected in four urban environments [23], [24] to create training and test sets to train and test the proposed DL model.
- Demonstration that the DL model can provide better prediction accuracy than traditional path loss models, and discussion of its generalization performance to new locations after fine-tuning.

The remainder of this paper is organized as follows. In Section II, we discuss related work found in the literature. In Section III, we describe our proposed model-aided DL approach for path loss prediction at 7 GHz. In Section IV, we provide details of the real measurement data, comparison with empirical models, and our workflow of the main tasks performed in this study. Then, we present numerical results during both training and generalization processes of the model in Section V. Finally, we summarize our results and provide concluding remarks in Section VI.

## II. LITERATURE REVIEW

Channel models play an important role in wireless communication system planning and interference assessment, particularly in spectrum sharing bands. Even though various path loss models have been studied and evaluated for different scenarios and at different frequencies within (0.5 to 100) GHz [3], [5], [6], choosing a relevant model for a particular area of interest within a frequency band is not always straightforward. Often, there is a trade-off between the desirable performance accuracy from a model and the computational complexity needed to achieve that level of accuracy. The studies in [5], [6] found that typical best-case performance accuracy from numerous path loss models is (12 to 15) dB root mean square error (RMSE). Some of the models that can be tuned or fitted with measurements can

further reduce the RMSE to (8 to 9) dB. Theoretical and empirical models are generally simple and computationally inexpensive, but they lack the capability to provide accurate prediction results. On the contrary, ray tracing models can provide more accurate path loss predictions in exchange for more intensive computational efforts [7]. An example of using 3D ray tracing method for indoor propagation loss prediction is presented in [8].

Given the significant development of ML and DL technology in recent years, researchers have leveraged these technologies to improve the performance accuracy of path loss models while trying to limit the computation complexity incurred. An overview of recent ML techniques, associated input features and output, used for propagation modeling is provided in [9]. The authors in [10] propose a feed-forward deep neural network model to predict path loss of different frequencies in (0.8 to 70) GHz in a mixed urban and suburban and in NLOS environment. Both studies in [11], [12] use principal component analysis to generate low-dimensional environmental features for the dataset, and then employ artificial neural networks to learn the path loss from the reduced dimension dataset. Another interesting approach proposed in [13] is to develop a DL encoder-decoder architecture to segment a satellite imagery of a given environment into three different classes (i.e., urban, suburban, and rural). Depending on the environmental class that each segment of the link falls into, an appropriate Okumura-Hata model is used to compute the path loss for that segment. Instead of predicting path loss for each link, the authors in [14] present a different approach to use the DL VGG-16 architecture to predict path loss distribution of an area from 2D satellite images.

The authors in [15] propose a simple ML framework, which uses terrain profile and distance between transmitter and receiver as features, for outdoor path loss prediction over irregular terrain. A more advanced framework using specialized 3D engineered features and deep neural networks to predict signal strength at the receiver is presented in [16]. Furthermore, the authors in [17] reformulate propagation modeling problem to an image regression problem by converting propagation parameters into image tensors and feeding them into a deep convolutional neural network (CNN). Similarly, the work in [18] manipulates and transforms the vectors of tabular data into images. These synthetic images are fused with images representing selected regions of the area's map and used as inputs to a CNN for path loss prediction. Unlike previous approaches, a long short-term memory neural network is proposed to predict path loss in (2 to 26) GHz band in [19]. Among many innovative ML and DL techniques, we found the approach proposed by [20] interesting and closely related to our work. The proposed model is a hybrid model which combines both a physics-based model and a correctional neural network for path loss prediction.

### III. MODEL-AIDED DEEP LEARNING APPROACH

We use a model-aided deep learning approach for path loss prediction at 7 GHz. The approach was first developed in [20] for 811 MHz and 2630 MHz bands, and adapted in [22] for 3.5 GHz band. Compared to previous models in [20], [22], the proposed model in this paper uses a slightly different set of input features (for both fundamental and engineered features) and predicts the path loss directly (instead of received signal strength). However, the proposed approach is still a hybrid model, which includes a physics-based model and a correctional neural network. We leverage both modeling-based and learning-based capabilities to obtain better performance accuracy for path loss prediction.

Fig. 1 shows the architecture of the proposed model-aided deep learning model. The model takes in three inputs:

- $\mathbf{x}_1 = [d, f_c, h_{TX}, h_{RX}]$ : fundamental features, where  $d$  is the 3D distance between the transmitter and receiver (km),  $f_c$  is the center frequency (GHz), and  $h_{TX}$  and  $h_{RX}$  are the respective transmitter and receiver heights (m),
- $\mathbf{x}_2 = [\text{lat}_{RX}, \text{lon}_{RX}, d, d_{lat}, d_{lon}]$ : engineered features, where  $\text{lat}_{RX}$  and  $\text{lon}_{RX}$  are the respective receiver coordinates in latitude and longitude,  $d$  is the 3D distance (km), and  $d_{lat}$  and  $d_{lon}$  are the respective distances in latitude and longitude between the transmitter and receiver,
- $A$ : satellite image, 256 pixel  $\times$  256 pixel ( $\approx 185$  m  $\times$  185 m), centered at the receiver location and rotated by an angle equal to the bearing between transmitter and receiver.

The final output of the DL model is the corrected path loss value  $p$  from the transmitter to each receiver location. The path loss  $p$  is the sum of the path loss estimate  $z$  (output from the physics-based model) and the correction  $y$  (output from the correctional neural network).

#### A. PHYSICS-BASED MODEL

The physics-based model provides domain expert knowledge to assist in predicting the path loss. We use the 3rd Generation Partnership Project (3GPP) empirical channel model in Urban Macro (UMa) scenario and NLOS condition [3] for our physics-based model. Table 3 in Section IV-B describes the equations and parameters of the 3GPP model in detail. We select the 3GPP model because it is a general purpose propagation model and it is applicable to a wide frequency range (0.5 to 100) GHz.

The input parameters to the physics-based model are the fundamental features  $\mathbf{x}_1$ , which include 3D distance  $d$ , center frequency  $f_c$ , transmitter height  $h_{TX}$  and receiver height  $h_{RX}$ . The output is the median path loss estimate  $z$  between the transmitter and receiver. In addition to serving as an intermediate result, the path loss estimate  $z$  will be concatenated with the engineered features  $\mathbf{x}_2$ , and then input to the correctional neural network to obtain a correction value  $y$ .

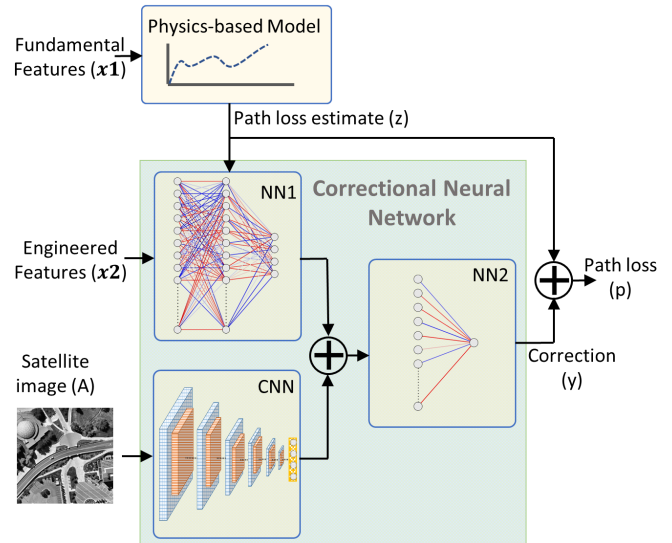


FIGURE 1. A model-aided deep learning architecture, which consists of a physics-based model and a correctional neural network, is used for predicting the path loss between the transmitter and receiver.

#### B. CORRECTIONAL NEURAL NETWORK

The correctional neural network, similar to the models presented in [20], [22], consists of three DL submodels. The architecture and configuration parameters of these submodels are demonstrated in Fig. 2. The first DL model (NN1) consists of three fully connected layers, as shown in Fig. 2(a). The input to this network is a concatenation of the engineered features  $\mathbf{x}_2$  and the path loss estimate  $z$ . The second DL model is a convolutional neural network (CNN), as shown in Fig. 2(b). The input to this model consists of grayscale satellite images  $A$ . The CNN model comprises six convolutional blocks, followed by a simple dense layer with linear activation. Each convolutional block includes a convolutional layer, a max pooling layer, LeakyReLU activation, and batch normalization. The outputs of NN1 and CNN are added together to form the input to the third deep learning model (NN2). The architecture of NN2 consists of two fully connected layers, as shown in Fig. 2(c). The single output of this model represents the correction factor  $y$  for the path loss.

The model is trained using a mean squared error (MSE) loss function and Adam optimizer. To reduce overfitting, weight decay is applied in addition to the batch normalization layers shown in Fig. 2. Image augmentation with random rotation angle relative to the original image orientation is also used to improve generalization. The random rotation angle is bounded by a maximum image augmentation angle. Furthermore, a relatively small mini-batch size is used to speed up the training process. The simulation hyperparameters are presented in Table 1.

#### IV. DATASET GENERATION

Besides using a good learning algorithm, we also need sufficient quantity and high quality data for training and testing the model. In this section, we describe the real propagation

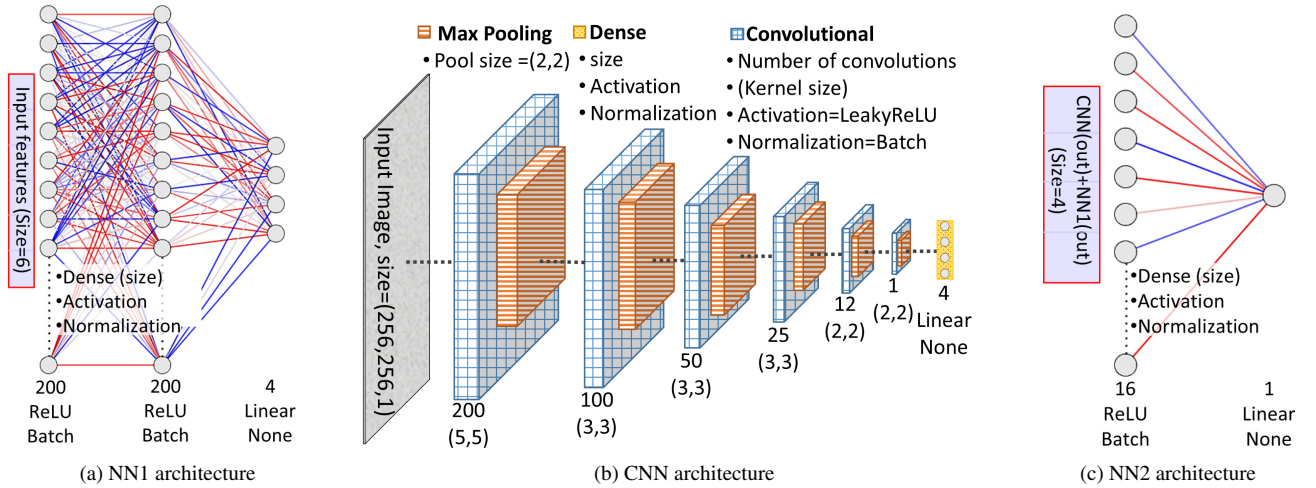


FIGURE 2. Detailed architectures and parameters of three sub-models within the correctional neural network model.

TABLE 1. Simulation Parameters Used to Train the Correctional Neural Network Model.

Parameter	Value
Batch size	8
Loss function	MSE
Optimizer	Adam
Weight decay	2.8e-3
Learning rate	1e-3
Max image augmentation angle	20°

measurement data collected in Colorado at 7 GHz and how we use them to generate the training set and test set.

### A. REAL PROPAGATION MEASUREMENT DATA

We utilize real propagation measurement data collected in four locations in mixed LOS/NLOS conditions in Boulder and Louisville, Colorado, during the winter. Path loss was measured in a light urban environment with residential buildings of up to five floors, commercial buildings of up to three floors, and trees. A continuous wave signal was transmitted at 18 dBm (dBm is power level expressed in decibels (dB) with reference to one milliwatt (mW)) and input to a horn antenna of 12 dBi gain located on top of a building. The half-power beamwidth (HPBW) of the antenna is 50° on the E-field and 40° on the H-field. The receiver was mobile, and an omnidirectional antenna of 3.4 dB was mounted on a car at 1.5 m above ground level. A low-noise amplifier (LNA) of 36.4 dB was used and the peak power level of the received signal was recorded using a spectrum analyzer. The total loss through cables and connectors was 9.4 dB.

The transmitter was placed at four locations, i.e., three at the University of Colorado Boulder and one on a roof of a two-story office building in Louisville, Colorado. Their antenna heights, azimuth angles, measurement radius and number of samples are indicated in Table 2. More information on the measurement campaign can be found in [24]. Fig. 3 shows the driving route within the HPBW of the transmit antenna considered for each scenario. The colors represent the path

loss values at each receiver location. Specifically, the path loss between a transmitter and a receiver can be computed as

$$PL = P_{TX} + G_{TX} - L_{CC} + G_{LNA} + G_{RX} - P_{RX} \quad (1)$$

where  $PL$  is the path loss (dB),  $P_{TX}$  is the transmitter power level (dBm),  $G_{TX}$  is the transmitter antenna gain (dBi),  $L_{CC}$  is the total loss of cables and connectors (dB),  $G_{LNA}$  is the low noise amplifier gain (dB),  $G_{RX}$  is the receiver antenna gain (dBi), and  $P_{RX}$  is the measured received power (dBm).

### B. COMPARISON WITH EMPIRICAL MODELS

The measurement data in each location have been compared with the empirical channel models indicated in Table 3, such as WINNER II [25] and 3GPP [3] in an Urban Macrocell environment. WINNER II is used in the cellular industry and, although is valid only up to 6 GHz, the FCC has suggested it for spectrum sharing analysis in the 6 GHz band [1]. The 3GPP channel model has been proposed for 5G and is valid up to 100 GHz. Our measurement data have also been compared with the floating intercept (FI) and close-in free space reference distance (CI) path loss models [26]. Parameters of the FI and CI models were previously calculated based on measurement data in all four locations with slightly different selected data points [24].

Fig. 4 compares the measured path loss (gray) in mixed LOS/NLOS conditions with these empirical models and the free space path loss for each scenario. Their performance is evaluated using the root mean square error (RMSE), which is computed as follows

$$RMSE = \sqrt{\frac{1}{m} \sum_{i=1}^m (PL_i - \widetilde{PL}_i)^2} \quad (2)$$

where  $i = 1, \dots, m$  is the index of the sample,  $m$  is the total number of samples,  $PL_i$  is the measured path loss (dB), and  $\widetilde{PL}_i$  is the predicted path loss from empirical models (dB).

Table 4 shows the RMSE performance of the empirical models. Their difference is due to the different scenarios and

TABLE 2. Transmitter Locations and Parameters

Location number	Location name	Height (m)	Azimuth angle	Measurement radius (km)	Number of samples
1	CU Boulder, engineering tower, 7th floor	27	197°	1.5	15 771
2	CU Boulder, engineering tower, 8th floor	33	0°	3.3	9 258
3	CU Boulder, University Memorial Center, 5th floor	17	122°	1.8	4 875
4	Two-story office building in Louisville	10	4°	2.5	35 700

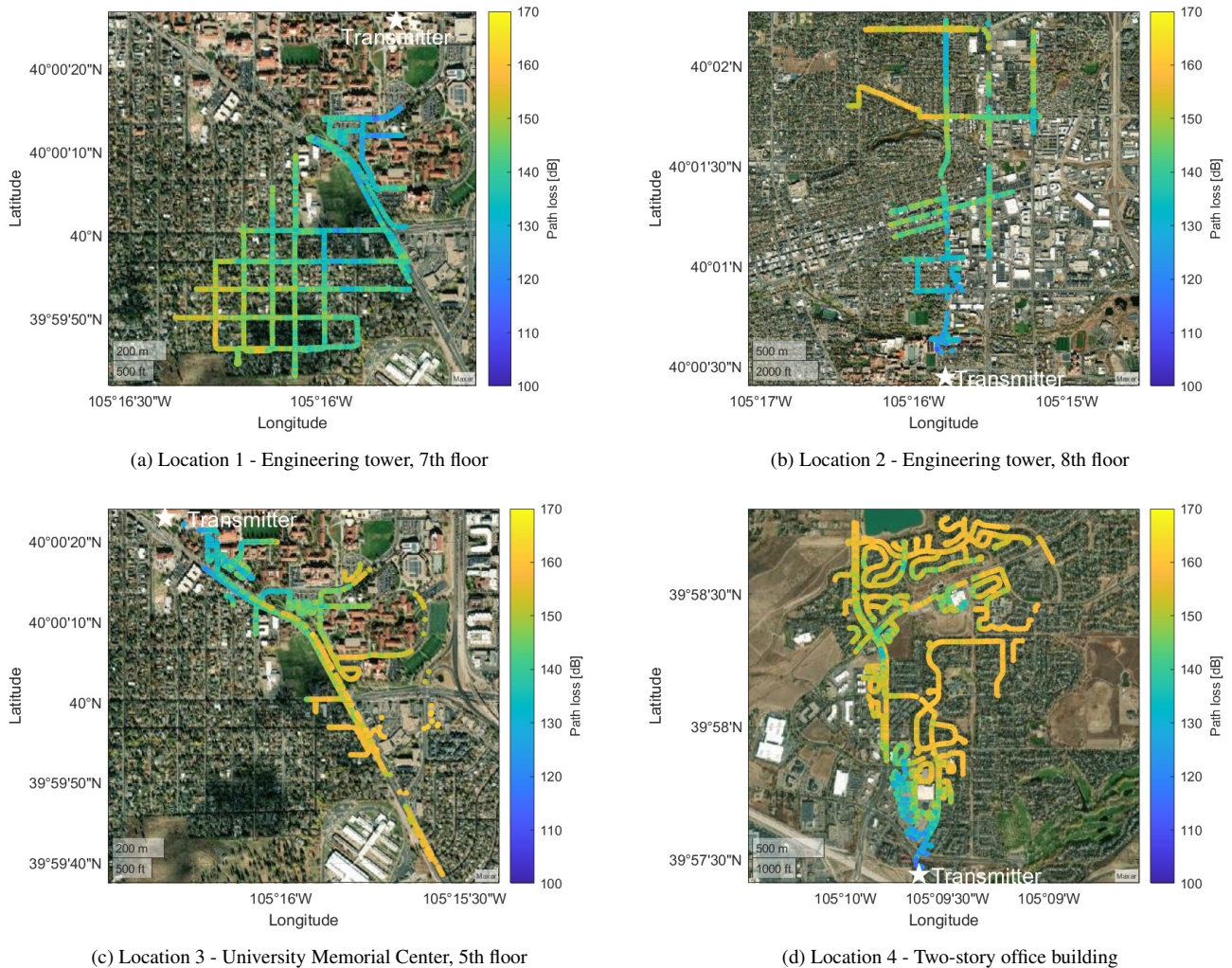


FIGURE 3. Path loss data collected in four locations in mixed LOS/NLOS conditions in Boulder and Louisville, Colorado.

antenna heights. Since the parameters used in the FI and CI models were calculated based on these measurements, we observe that they provide the best fit to the data. The FI model provides the lowest RMSE, because it is purely based on a least-squares linear regression of the measured data, while the CI model has a physical reference point that corresponds to the free space path loss at a distance  $d_0$ , in our case,  $d_0 = 1$  m. For the WINNER II and 3GPP models, NLOS conditions provide significantly lower RMSE than LOS, which indicates that most of the data points correspond to NLOS. The only exception is when the transmitter is on the 8th floor in location 2, which is the highest transmitter

location, and it caused an increased number of LOS data points along the driving path.

### C. WORKFLOW

We summarize the end-to-end workflow of our study in Fig. 5. Our first task is to get sufficient quantity and good quality data to train and test the path loss prediction model at 7 GHz. We utilize the real propagation measurement data collected in four locations in Boulder and Louisville, Colorado, as described in Section IV-A. We then use MATLAB and Python to pre-process the raw data in order to extract relevant features and targets for the model and save them in

TABLE 3. 7 GHz Path Loss Models for Urban Environment

Path loss model	Condition	Path loss (dB)	Distance
Floating-intercept	LOS	$73.2 + 20.3 \log_{10}(d)$	100 m < $d$ < 5 km
	NLOS	$74.7 + 20.4 \log_{10}(d)$	
Close-in	LOS	$49.3 + 27.5 \log_{10}(d)$	1 m < $d$ < 5 km
	NLOS	$49.3 + 28.5 \log_{10}(d)$	
WINNER II	LOS	$39 + 26 \log_{10}(d) + 20 \log_{10}(f_c/5)$	10 m < $d \leq d_{BP}$
		$40 \log_{10}(d) + 13.47 - 14 \log_{10}(h_{TX} - 1) - 14 \log_{10}(h_{RX} - 1) + 6 \log_{10}(f_c/5)$	$d_{BP} < d < 5$ km
	NLOS	$(44.9 - 6.55 \log_{10}(h_{TX})) \log_{10}(d) + 34.46 + 5.83 \log_{10}(h_{TX}) + 23 \log_{10}(f_c/5)$	50 m < $d$ < 5 km
3GPP	LOS	$28 + 22 \log_{10}(d) + 20 \log_{10}(f_c)$	10 m < $d_{2D} \leq d_{BP}$
		$28 + 40 \log_{10}(d) + 20 \log_{10}(f_c) - 9 \log_{10}((d_{BP})^2 + (h_{TX} - h_{RX})^2)$	$d_{BP} < d_{2D} < 5$ km
	NLOS	$\max(PL_{LOS}, PL'_{NLOS}),$ $PL'_{NLOS} = 13.54 + 39.08 \log_{10}(d) + 20 \log_{10}(f_c) - 0.6(h_{RX} - 1.5)$	10 m < $d_{2D} < 5$ km

Where:  
 $f_c$ : center frequency (GHz);  $c = 3 \times 10^8$  (m/s) is the propagation velocity in free space;  
 $h_{TX}$ : transmitter (TX) antenna height (m);  $h_{RX}$ : receiver (RX) antenna height (m);  $d$ : 3D TX-RX separation (m);  $d_{2D}$ : 2D TX-RX separation (m);  
 Break-point distance  $d_{BP} = 4(h_{TX} - 1)(h_{RX} - 1)f_c * 10^9 / c$ , assuming an effective environment height of 1 m for urban macrocell (UMa)

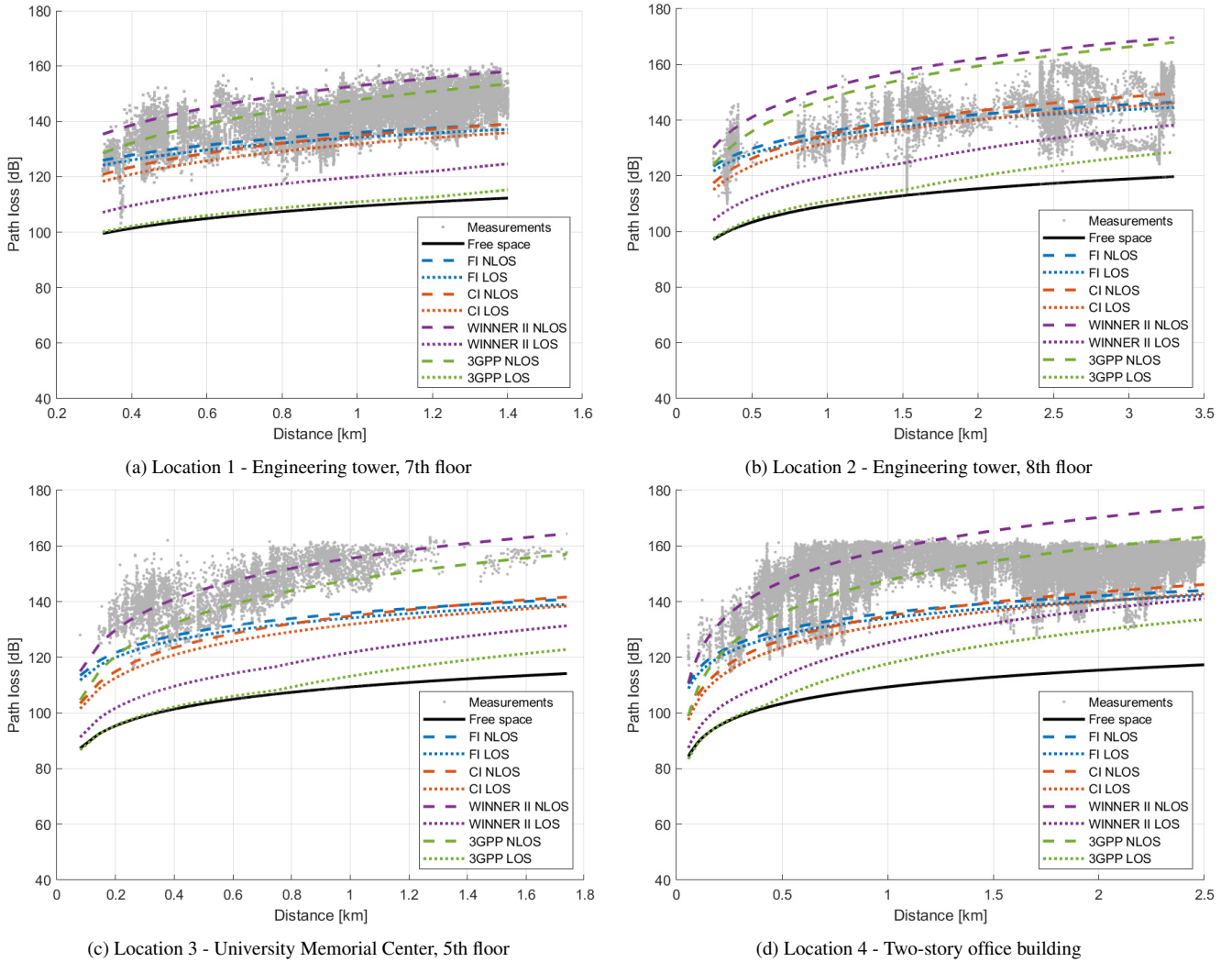


FIGURE 4. Real measurement data vs. predicted path loss from empirical models.

**TABLE 4.** RMSE Path Loss Performance of Empirical Models (dB)

Propagation model	Condition	Location 1	Location 2	Location 3	Location 4
Floating-intercept	LOS	9.6	9.5	17.2	16.1
	NLOS	8.3	9.7	15.5	14.4
Close-in	LOS	11.5	9.5	20.8	17.5
	NLOS	9.2	9.8	18.1	14.8
WINNER II	LOS	22.3	14.5	31.5	22.6
	NLOS	12.6	22.9	6.1	15.1
3GPP	LOS	30.8	22.3	39.3	29.7
	NLOS	8.5	20.6	9	8.9

.csv files. In addition, we generate satellite images centered at the receiver locations by using the Mapbox tool through its web services API. We combine these satellite images with the features and targets files to create a training set and a test set. For the training set, we further split it into a smaller training set and a validation set, and then train the model against the smaller training set and evaluate it against the validation set. After the model is trained, we use the test set to fine-tune and evaluate the prediction performance of the model. Model training, testing, and performance evaluation tasks are performed in PyTorch.

## V. RESULTS

In this section, we present results of the path loss prediction at 7 GHz in an urban environment using the proposed model-aided deep learning model, which is also preferred to as a neural network (NN) model for short. We first describe the training and evaluation on the training set, and then discuss the generalization performance of the trained model on the test set. We carefully partition the measurement data collected in different locations for the training set and the test set, so that we can demonstrate how well the trained model is able to predict unseen data.

### A. TRAINING AND EVALUATING THE MODEL ON THE TRAINING SET

We select the measurement data collected in location 1 (CU Boulder, engineering tower, 7th floor) as the training set. This location has the largest number of samples among the three CU Boulder locations, thus, it can provide sufficient quantity of training data. Although location 4 (two-story office building in Louisville) has the most samples, we reserve the measurement data at this location for the testing set, so that we can assess the trained model performance at another location outside of CU Boulder campus.

Fig. 6 shows the training route and validation route (left subplot) and the path loss vs. distance of the training and validation sets (right subplot). Out of 15 771 collected data samples, we separate 12 810 samples for a smaller training set and use the remaining 2 961 samples for the validation set. The training route covers an area within the HPBW of the transmitter antenna and about 0.3 km to 1.4 km away from it. The validation route is much shorter within 0.5 km to 1 km away from the transmitter. A few training samples appear on

the validation route due to redundant data collection during the measurement campaign.

Optimizing the neural network architecture and hyperparameters is a challenging task due to the large search space and lack of principled approaches. A successful optimization requires a combination of traditional grid search, heuristic methods (such as genetic algorithms or Bayesian optimization), and expert knowledge. In this work, we use a combination of traditional grid search and expert knowledge to come up with a model that provides good performance. Specifically, we implemented and trained several architectures of the correctional neural network, varying the NN1, CNN, and NN2 configurations in terms of larger and smaller architecture settings. Larger architecture configurations refer to more layers and units, while smaller architecture configurations refer to fewer layers and units. We also varied some of the model's hyperparameters. The best performance we found, in terms of normalized MSE loss during training and validation, was for models with the architecture and parameters presented in Fig. 2 and Table 1.

The final correctional neural network model was trained and validated using 50 epochs. Fig. 7 depicts the normalized MSE loss at each epoch during training and validation. As the number of epochs increases, the normalized MSE loss for training process gradually decreases and reaches a stable value below 0.3. On the other hand, the normalized MSE loss for the validation process also trends downward but its value is about 0.05 higher than the training loss. To reduce severe overfitting, we used data augmentation and tuned regularization parameters during training.

Our next step is to analyze the prediction performance on the validation set. Fig. 8 shows the path loss vs. distance prediction results of the proposed NN (blue) as well as the physics-based model (green) against the validation set (orange). Recall that the physics-based model is the 3GPP model in UMa scenario and NLOS condition. While the physics-based model tends to give higher predictions than the validation data, the NN provides predictions closer to the targets. To compare the predictive performance of the NN and the physics-based models, we compute the RMSE, which is a typical performance measure for regression problems. A smaller RMSE value indicates a closer prediction to the target. As expected, the NN model provides a very good RMSE value of 4.5 dB, whereas the physics-based model gives a higher RMSE value of 8.6 dB. Although in this scenario both models have RMSE scores below or within the range of (8 to 9) dB achieved by tuned or fitted models described in [5], [6], leveraging the learned correction using engineered features and satellite images, the NN is able to predict the target more accurately than the physics-based model alone.

### B. GENERALIZATION PERFORMANCE ON THE TEST SET

Having the NN model trained on the training set collected in location 1, we evaluate the model on a test set, which com-

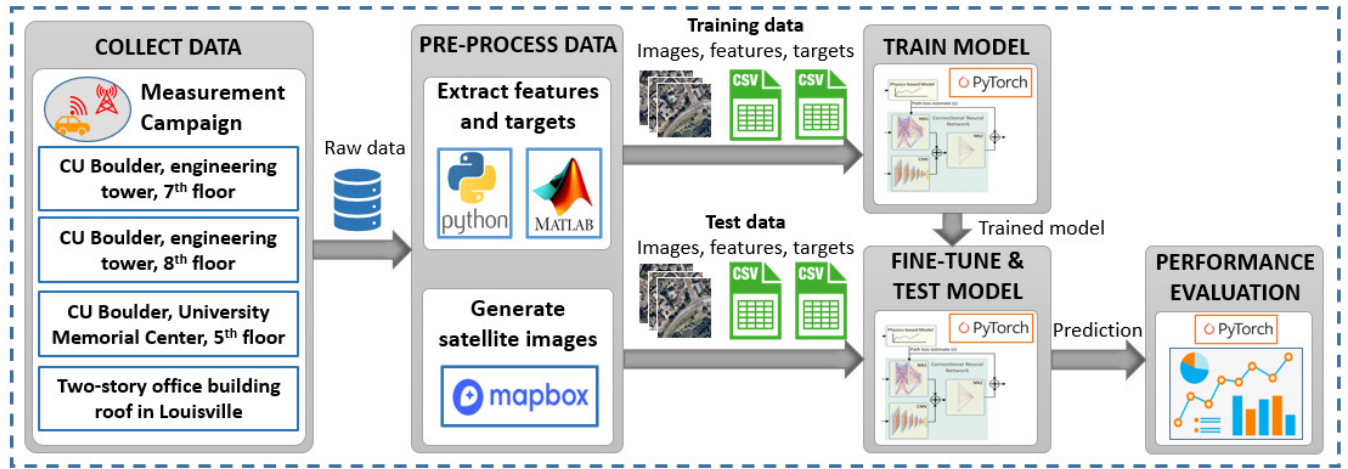


FIGURE 5. Workflow summarizing main tasks performed in this study including data collection, data pre-processing, model training, testing, and performance evaluation.

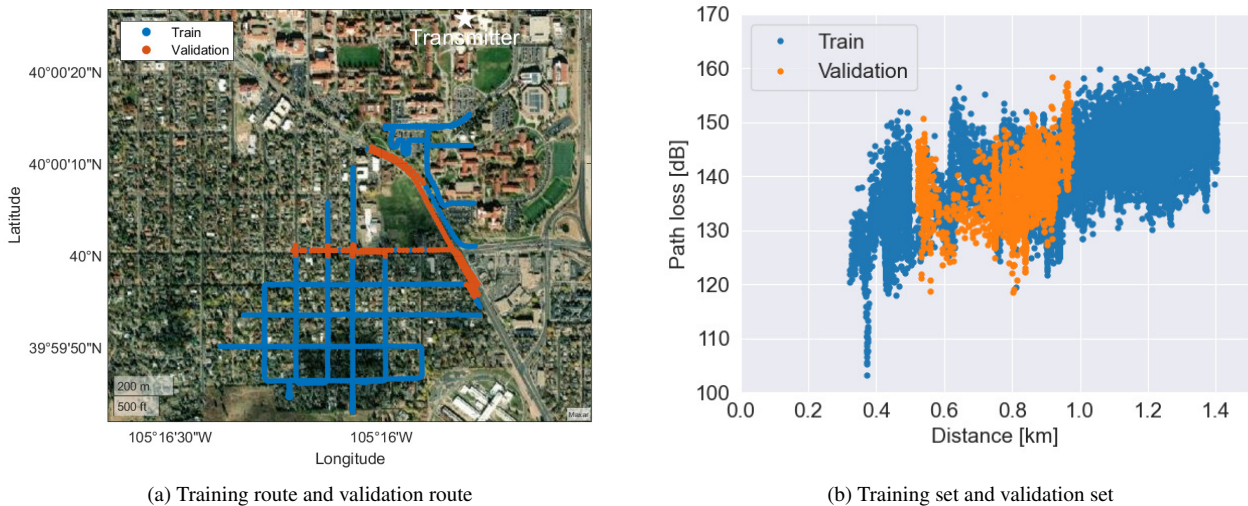


FIGURE 6. Training and validation routes and datasets extracted from measurement data in location 1.

prises of measurements collected in location 2 (CU Boulder, engineering tower, 8th floor), location 3 (CU Boulder, University Memorial Center, 5th floor), and location 4 (two-story office building in Louisville). By analyzing the generalization error, i.e., the error rate on new cases, we gain insight into how well the model will perform on new data.

Since the data in the training and validation sets were collected at different locations with different measurement settings (e.g., different transmitter heights and antenna azimuth angles), they might not be perfectly representative of the data in the test set. To mitigate the data mismatch problem, for each test location, we hold out 10% of the test set to fine-tune the model by retraining and then test the newly trained model against the remaining 90% of the test set. Fig. 9 shows the path loss prediction vs. distance of the proposed NN model (blue) and of the physics-based model (green) against the test set (orange) at each location. Table 5 shows the generalization errors in terms of RMSE

TABLE 5. Generalization Performance at Three Test Locations.

Location number	Neural network RMSE performance (dB)	Physics-based RMSE performance (dB)
2	4.5	20.6
3	4.9	9
4	4.3	8.9

for both the NN model and the physics-based model at these locations. The NN outperforms the physics-based model as its predictions are much closer to the test set with RMSE values below 5 dB for all cases. In contrast, the physics-based model provides higher RMSE values around 9 dB and it overestimates the path loss in location 2. These values are the same as those shown in the last row of Table 4 for the 3GPP model in NLOS condition.

To examine how well the trained model performs with less fine-tuning data, we vary the ratio of data used for fine-tuning and testing the NN, and then observe the predictive

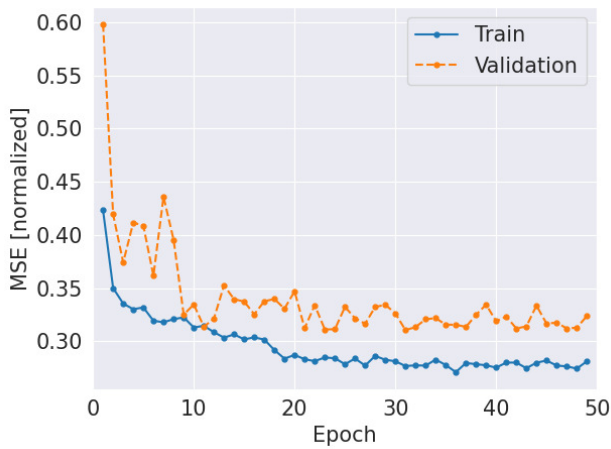
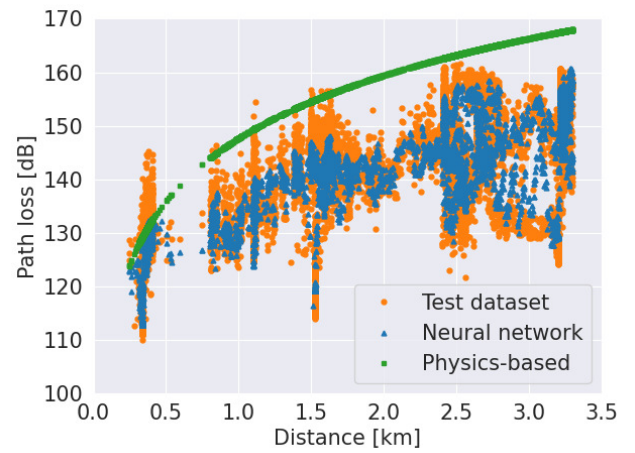
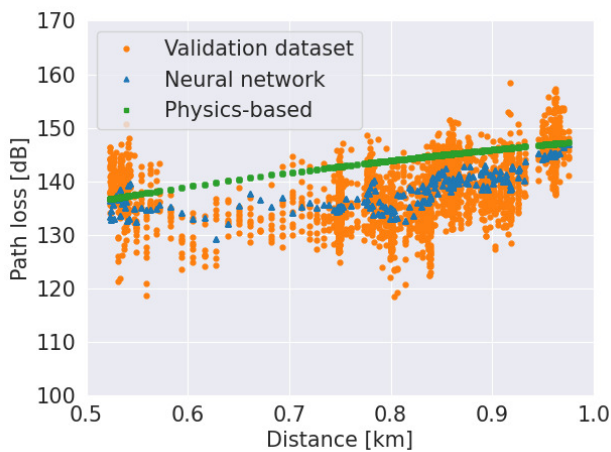


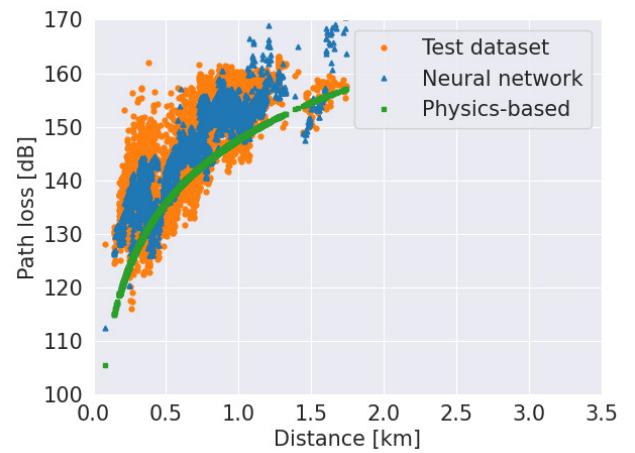
FIGURE 7. Normalized mean square error (MSE) loss during training and validation of the deep learning model.



(a) Location 2



(b) Location 3



(c) Location 4

FIGURE 8. Prediction results of the neural network and physics-based models on the validation set.

performance. Fig. 10 shows the RMSE performance for three sets of (fine-tune, test) ratios at each location. Without fine-tuning, i.e., (fine-tune, test) = (0 %, 100 %), the NN does not perform well, especially in location 2. However, as the ratio of fine-tuning data increases to 5 %, the RMSE values drop significantly, around 5 dB, for all locations. And when (fine-tune, test) = (10 %, 90 %), the RMSE values decrease further, but with negligible changes, for all locations. In summary, the results show that the NN model, which was trained with measurement data in a particular location, may not immediately perform well at other locations. Nevertheless, after fine-tuning with a reasonable amount of new data, the performance of the NN model can be improved at other locations.

To evaluate the effectiveness of the initial training procedure, we tested the performance of the neural network model using default randomized parameters on measurements collected from different test locations. The RMSE results, as

FIGURE 9. Generalization performance of the neural network model at three test locations.

presented in Fig. 11, demonstrate that the model trained from scratch performs almost comparably to the pretrained model

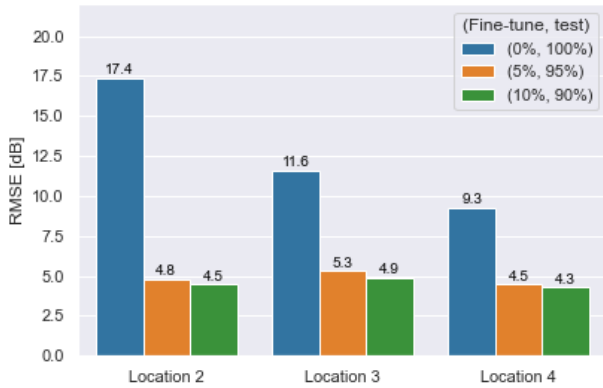


FIGURE 10. Generalization performance of the neural network with different ratios of (fine-tune, test) at three test locations.

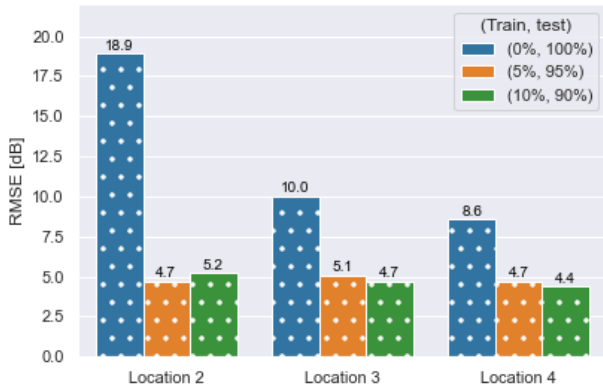


FIGURE 11. Prediction performance of the neural network with different ratios of (train, test) at three test locations.

in Fig. 10. Therefore, the generalization capability of the model to new locations remains uncertain and requires further investigation. Obtaining additional data from various locations may assist in capturing the environmental and terrain diversity, which could improve the model’s generalization performance.

VI. CONCLUSION

We found that the model-aided deep learning technique can provide better accuracy for path loss prediction than most traditional models at 7 GHz in an urban environment. The RMSE performance of the trained and fine-tuned models is within (4 to 5) dB range, which is more desirable than the (8 to 9) dB range achieved by tuned or fitted models [5], [6]. Although the learning knowledge provided by the correctional neural network plays an important role in lowering the RMSE values, its main drawback is the computational complexity during the offline training process.

For future work, we plan to update the physics-based model with the hybrid propagation model developed by the WinnForum. We also investigate the performance effects of

the model with and without using a large amount of satellite images as input. Furthermore, we will extract 3D features, e.g., building and vegetation heights, along the propagation path and incorporate these features into the model to further improve the performance accuracy. In addition, we will test the model with data in other frequency bands (e.g., 13 GHz) to ensure the robustness and accuracy of the work. Finally, we will implement and compare the performance of our model with other ray tracing models and ML/DL approaches.

NOTATION

Model-aided deep learning parameters

$x_1$	Vector of fundamental features
$d$	3D distance from transmitter to receiver
$f_c$	Center frequency
$h_{TX}$	Transmitter height
$h_{RX}$	Receiver height
$x_2$	Vector of engineered features
$lat_{RX}$	Receiver latitude coordinate
$lon_{RX}$	Receiver longitude coordinate
$d_{lat}$	Distance in latitude
$d_{lon}$	Distance in longitude
$A$	Satellite image
$z$	Path loss estimate
$y$	Correction
$p$	Corrected path loss

Link budget parameters

$PL$	Path loss
$P_{TX}$	Transmitter power level
$G_{TX}$	Transmitter antenna gain
$L_{CC}$	Total loss of cables and connectors
$G_{LNA}$	Low noise amplifier gain
$G_{RX}$	Receiver antenna gain
$P_{RX}$	Measured received power

ACKNOWLEDGMENT

The authors thank the National Telecommunications and Information Administration (NTIA), Institute for Telecommunication Sciences (ITS) for providing the equipment used in the measurement data and the University of Colorado Boulder for permitting access to the transmit locations.

REFERENCES

- [1] FCC, “Unlicensed use of the 6 GHz band; Expanding flexible use in mid-band spectrum between 3.7 and 24 GHz,” FCC-20-51, Apr. 24, 2020.
- [2] WinnForum Standards, “Functional requirements for the U.S. 6 GHz band under the control of an AFC system,” WINNF-TS-1014, version V1.2.1, Release 10, Nov. 2022.
- [3] ETSI, “5G; Study on channel model for frequencies from 0.5 to 100 GHz,” 3GPP TR 38.901, version 16.1.0, Release 16, Nov. 2020.
- [4] ITU, “Guidelines for evaluation of radio interface technologies for IMT-2020,” Report ITU-R M.2412-0, Oct., 2017.
- [5] C. Phillips, D. Sicker, and D. Grunwald, “Bounding the error of path loss models,” in *Proc. IEEE DySPAN*, Aachen, Germany, 2011, pp. 71–82.
- [6] C. Phillips, D. Sicker, and D. Grunwald, “A survey of wireless path loss prediction and coverage mapping methods,” *IEEE Commun. Surv. Tutor.*, vol. 15, no. 1, pp. 255–270, First Quarter 2013.

- [7] Z. Yun, and M. F. Iskander, "Ray tracing for radio propagation modeling: principles and applications," *IEEE Access*, vol. 3, pp. 1089–1100, Jul. 2015.
- [8] T. K. Geok, F. Hossain, S. K. A. Rahim, O. Elijah, A. A. Eteng, C. T. Loh, L. L. Li, C. P. Tso, T. A. Rahman, and M. N. Hindia, "3D RT adaptive path sensing method: RSSI modelling validation at 4.5 GHz, 28 GHz, and 38 GHz," *Alexandria Eng.*, vol. 61, no. 12, pp. 11041–11061, Dec. 2022.
- [9] A. Seretis and C. D. Sarris, "An overview of machine learning techniques for radiowave propagation modeling," *IEEE Trans. Antennas Propag.*, vol. 70, no. 6, pp. 3970–3985, June 2022.
- [10] C. Nguyen and A. A. Cheema, "A deep neural network-based multi-frequency path loss prediction model from 0.8 GHz to 70 GHz," *Sensors*, 21, 5100, Jul. 2021.
- [11] L. Wu, D. He, B. Ai, J. Wang, H. Qi, K. Guan, and Z. Zhong, "Artificial neural network based path loss prediction for wireless communication network," *IEEE Access*, vol. 8, pp. 199523–199538, Nov. 2020.
- [12] H.-S. Jo, C. Park, E. Lee, H. K. Choi, and J. Park, "Path loss prediction based on machine learning techniques: Principal component analysis, artificial neural network and Gaussian process," *Sensors*, 20(7):1927, Mar. 2020.
- [13] M. E. Morocho-Cayamcela, M. Maier, and W. Lim, "Breaking wireless propagation environmental uncertainty with deep learning," *IEEE Trans. Wireless Commun.*, vol. 19, no. 8, pp. 5075–5087, Aug. 2020.
- [14] O. Ahmadien, H. F. Ates, T. Baykas, and B. K. Gunturk, "Predicting path loss distribution of an area from satellite images using deep learning," *IEEE Access*, vol. 8, no. 1, pp. 64982–64991, 2020.
- [15] M. Ribero, R. W. Heath Jr., H. Vikalo, D. Chizhik, and R. A. Valenzuela, "Deep learning propagation models over irregular terrain," in *Proc. IEEE ICASSP*, Brighton, UK, pp. 4519–4523, 2019.
- [16] U. Masood, H. Farooq, and A. Imran, "A machine learning based 3D propagation model for intelligent future cellular networks," in *Proc. IEEE GLOBECOM*, Waikoloa, HI, USA, pp. 1–6, 2019.
- [17] X. Zhang, X. Shu, B. Zhang, J. Ren, L. Zhou, and X. Chen, "Cellular network radio propagation modeling with deep convolutional neural networks," in *Proc. IEEE 26th ACM SIGKDD*, pp. 2378–2386, 2020.
- [18] S. P. Sotiroidis, P. Sarianniadis, S. K. Goudos, and K. Siakavara, "Fusing diverse input modalities for path loss prediction: a deep learning approach," in *IEEE Access*, vol. 9, pp. 30441–30451, 2021.
- [19] M. Sasaki, N. Kuno, T. Nakahira, M. Inomata, W. Yamada, and T. Moriyama, "Deep learning based channel prediction at 2–26 GHz band using long short-term memory network," in *Proc. IEEE 15th EuCAP*, pp. 1–5, 2021.
- [20] J. Thrane, D. Zibar, and H. L. Christiansen, "Model-aided deep learning method for path loss prediction in mobile communication systems at 2.6 GHz," *IEEE Access*, vol. 8, pp. 7925–7936, 2020.
- [21] J. Thrane, B. Sliwa, C. Wietfeld, and H. L. Christiansen, "Deep learning-based signal strength prediction using geographical images and expert knowledge," in *Proc. IEEE GLOBECOM*, Taipei, Taiwan, Dec 2020.
- [22] T. T. Nguyen, R. Caromi, K. Kallas, and M. R. Souryal, "Deep learning for path loss prediction in the 3.5 GHz CBRS spectrum band," in *Proc. IEEE WCNC*, Austin, TX, USA, Apr. 2022.
- [23] N. Yoza-Mitsuishi and R. Sun, "Path loss characterization of 7-GHz terrestrial propagation channel in urban environment," in *Proc. IEEE 90th VTC Fall*, Honolulu, Hawaii, USA, Sept. 2019, pp. 1–5.
- [24] N. Yoza-Mitsuishi, C. R. Anderson, and P. Mathys, "Propagation model analysis for 7 and 13 GHz spectrum sharing in urban environment," *IEEE Wireless Commun. Lett.*, vol. 11, no. 9, pp. 1965–1969, Sept. 2022.
- [25] P. Kyösti *et al.*, "WINNER II channel models," Tech. Rep. IST-4-027756 WINNER II D1.1.2 V1.2, 2007.
- [26] S. Sun, T. S. Rappaport, S. Rangan, T. A. Thomas, A. Ghosh, I. Z. Kovacs, I. Rodriguez, O. Koymen, A. Partyka, and J. Jarvelainen, "Propagation path loss models for 5G urban micro- and macro-cellular scenarios," in *Proc. IEEE 83rd VTC Spring*, Nanjing, China, May 2016.



communications, cognitive radio, spectrum sharing, and machine learning and deep learning technologies.



NADIA YOZA-MITSUISHI received her B.S. degree from the Pontifical Catholic University of Peru and her M.S. and Ph.D. degrees from the University of Colorado Boulder. She previously worked as a wireless intern at CableLabs. Since 2021, she has been with the Communications Technology Laboratory (CTL) at the National Institute of Standards and Technology (NIST). Her research interests are wireless communications, spectrum sharing and propagation modeling.



RAIED CAROMI received the B.Sc. and M.Sc. degrees in electrical engineering from University of Mosul, Iraq, in 1999 and 2002, and the Ph.D. in systems engineering from the University of Arkansas at Little Rock (UALR) in 2014. He was a teaching assistance from 2010 to 2014 at College of Engineering, UALR. In 2013, he worked as an engineering intern at WINLAB/ Rutgers University, NJ. Since 2015, he has been with Communications Technology Laboratory (CTL) at the National Institute of Standards and Technology (NIST), Gaithersburg, MD. His research interests include cognitive radio, spectrum sharing, RF datasets generation and applications of machine learning in the next generation wireless communications.

...